Guided Growth of Millimeter-Long Horizontal Nanowires with Controlled Orientations

David Tsivion *et al.*

Science **333**, 1003 (2011);
DOI: 10.1126/science.1208455

Science (print ISSN 0036-8075; online ISSN 1095-9203) is published weekly, except the last week in December, by the American Association for the Advancement of Science, 1200 New York Avenue NW, Washington, DC 20005.

STM imaging (*29*, *32*, *38*). We performed STM spectroscopic mapping in a 2.5-nm area around one graphitic N dopant (STM junction parameters are $V = 0.8$ V, $I = 1$ nA). Shown in Fig. 4B are a subset of these maps, acquired at bias voltages (applied to the sample relative to the tip) from –0.78 to 0.78 V. The maps did not show much contrast at high positive bias, but the local DOS around the N atom was strongly suppressed at energies below the E_F. The local DOS recovered its background value within a few lattice constants of the dopant atom. We plotted the radial distribution of the dI/dV intensity (Fig. 4C) from the maps in Fig. 4B as a function of distance from the N atom, normalizing the background value of the dI/dV to unity for each energy. The intensity of the spectral weight changes caused by the N dopant were energy-dependent, but the decay lengths were ~7 Å for all energies (Fig. 4D). This result indicates that the electronic perturbation caused by a nitrogen dopant is localized near the dopant atom, which is confirmed in large-area dI/dV maps, and seen in the calculated charge distribution [see SOM II (e) and fig. S5] and simulated STM image in Fig. 2B (*26*).

References and Notes

1. N. W. Ashcroft, N. D. Mermin, *Solid State Physics* (Holt, New York, 1976).
2. A. H. Castro Neto, F. Guinea, N. M. R. Peres, K. S. Novoselov, A. K. Geim, *Rev. Mod. Phys.* **81**, 109 (2009).
3. X. R. Wang *et al.*, *Science* **324**, 768 (2009).
4. I. Gierz, C. Riedl, U. Starke, C. R. Ast, K. Kern, *Nano Lett.* **8**, 4603 (2008).
5. D. C. Wei *et al.*, *Nano Lett.* **9**, 1752 (2009).
6. Y.-C. Lin, C.-Y. Lin, P.-W. Chiu, *Appl. Phys. Lett.* **96**, 133110 (2010).
7. L. S. Panchokarla *et al.*, *Adv. Mater.* **21**, 4726 (2009).
8. Z. Z. Sun *et al.*, *Nature* **468**, 549 (2010).
9. D. Deng *et al.*, *Chem. Mater.* **23**, 1188 (2011).
10. L. T. Qu, Y. Liu, J. B. Baek, L. M. Dai, *ACS Nano* **4**, 1321 (2010).
11. Y. Wang, Y. Y. Shao, D. W. Matson, J. H. Li, Y. H. Lin, *ACS Nano* **4**, 1790 (2010).
12. J. C. Meyer *et al.*, *Nat. Mater.* **10**, 209 (2011).
13. X. Li *et al.*, *Science* **324**, 1312 (2009); 10.1126/science.1171245.
14. A. C. Ferrari *et al.*, *Phys. Rev. Lett.* **97**, 187401 (2006).
15. M. S. Dresselhaus, A. Jorio, A. G. Souza Filho, R. Saito, *Philos. Trans. R. Soc. A Math. Phys. Eng. Sci.* **368**, 5355 (2010).
16. A. Jorio *et al.*, *J. Phys. Condens. Matter* **22**, 334204 (2010).
17. M. M. Lucchese *et al.*, *Carbon* **48**, 1592 (2010).
18. J. Yan, Y. B. Zhang, P. Kim, A. Pinczuk, *Phys. Rev. Lett.* **98**, 166802 (2007).
19. A. Das *et al.*, *Nat. Nanotechnol.* **3**, 210 (2008).
20. I. Shimoyama, G. Wu, T. Sekiguchi, Y. Baba, *Phys. Rev. B* **62**, R6053 (2000).
21. N. Hellgren *et al.*, *Thin Solid Films* **471**, 19 (2005).
22. N. Hellgren *et al.*, *Appl. Phys. Lett.* **79**, 4348 (2001).
23. X. Li *et al.*, *J. Am. Chem. Soc.* **131**, 15939 (2009).
24. S. Point, T. Minea, B. Bouchet-Fabre, A. Granier, G. Turban, *Diamond Relat. Mater.* **14**, 891 (2005).
25. M. Endo, T. Hayashi, S. H. Hong, T. Enoki, M. S. Dresselhaus, *J. Appl. Phys.* **90**, 5670 (2001).
26. B. Zheng, P. Hermet, L. Henrard, *ACS Nano* **4**, 4165 (2010).
27. J. Tersoff, D. R. Hamann, *Phys. Rev. B* **31**, 805 (1985).
28. P. Giannozzi *et al.*, *J. Phys. Condens. Matter* **21**, 395502 (2009).
29. G. M. Rutter *et al.*, *Science* **317**, 219 (2007).
30. E. Cockayne *et al.*, *Phys. Rev. B* **83**, 195425 (2011).
31. Y. B. Zhang *et al.*, *Nat. Phys.* **4**, 627 (2008).
32. Y. B. Zhang, V. W. Brar, C. Girit, A. Zettl, M. F. Crommie, *Nat. Phys.* **6**, 74 (2010).
33. G. H. Li, A. Luican, E. Y. Andrei, *Phys. Rev. Lett.* **102**, 176804 (2009).
34. A. Lherbier, X. Blase, Y. M. Niquet, F. Triozon, S. Roche, *Phys. Rev. Lett.* **101**, 036808 (2008).
35. G. Giovannetti *et al.*, *Phys. Rev. Lett.* **101**, 026803 (2008).
36. P. A. Khomyakov *et al.*, *Phys. Rev. B* **79**, 195425 (2009).
37. K. S. Kim *et al.*, *Nature* **457**, 706 (2009).
38. A. Deshpande, W. Bao, F. Miao, C. N. Lau, B. J. LeRoy, *Phys. Rev. B* **79**, 205411 (2009).

Acknowledgments: This material is based on work supported as part of the Center for Re-Defining Photovoltaic Efficiency Through Molecule Scale Control, an Energy Frontier Research Center funded by the U.S. Department of Energy (DOE), Office of Science, Office of Basic Energy Sciences under award no. DE_SC0001085. Support was also provided by the Air Force Office of Scientific Research under grant no. FA9550-11-1-0010 (A.N.P); by the DOE under grants DE-FG02-88ER13937 (G.W.F) and DE-FG02-07ER15842 (T.H.) for research carried out in part at the Center for Functional Nanomaterials, Brookhaven National Laboratory, contract no. DE-AC02-98CH10886 (M.S.H.) and at the National Synchrotron Light Source, contract no. DE-AC02-98CH10886; by the Office of Naval Research under Graphene Multidisciplinary University Research Initiative (A.P. and P.K.); by the Defense Advanced Research Projects Agency Carbon Electronics for RF Applications program (P.K.); by the NSF under grant no. CHE-0641523 (A.P.); by the New York State Office of Science, Technology and Academic Research and by the Priority Research Centers Program (2011-0018395) through the National Research Foundation of Korea funded by the Ministry of Education, Science and Technology (K.S.K.). Equipment and material support was provided by the NSF under grant CHE-07-01483 (G.W.F.). Portions of this research were carried out at the Stanford Synchrotron Radiation Lightsource (SSRL), a Directorate of SLAC National Accelerator Laboratory and an Office of Science User Facility operated for the DOE Office of Science by Stanford University. We thank C. Jaye and D. Fischer for assistance in using National Synchrotron Light Source beamline U7A, H. Ogasawara for assistance at SSRL beamline 13-2, and C. Marianetti and D. Prezzi for useful discussions. The authors declare no competing financial interests. Requests for materials should be addressed to A.N.P.

Supporting Online Material

www.sciencemag.org/cgi/content/full/333/6045/999/DC1
Materials and Methods
SOM Text
Figs. S1 to S7

23 May 2011; accepted 29 June 2011
10.1126/science.1208759

Guided Growth of Millimeter-Long Horizontal Nanowires with Controlled Orientations

David Tsivion,[1] Mark Schvartzman,[1] Ronit Popovitz-Biro,[2] Palle von Huth,[2] Ernesto Joselevich[1]*

The large-scale assembly of nanowires with controlled orientation on surfaces remains one challenge preventing their integration into practical devices. We report the vapor-liquid-solid growth of aligned, millimeter-long, horizontal GaN nanowires with controlled crystallographic orientations on different planes of sapphire. The growth directions, crystallographic orientation, and faceting of the nanowires vary with each surface orientation, as determined by their epitaxial relationship with the substrate, as well as by a graphoepitaxial effect that guides their growth along surface steps and grooves. Despite their interaction with the surface, these horizontally grown nanowires display few structural defects, exhibiting optical and electronic properties comparable to those of vertically grown nanowires. This paves the way to highly controlled nanowire structures with potential applications not available by other means.

Semiconductors with controlled structures are at the core of the most advanced technologies in our everyday life, but defects induced by stress during growth often degrade the electronic and optical properties. For example, single-crystal gallium nitride was first produced in 1969 by epitaxial growth on sapphire (*1*), but it took three decades of research to reduce its defect concentration before it became the basis of the blue light-emitting diodes (LEDs) and violet lasers that enabled outdoor TV screens and the Blu-ray disk. The vapor-liquid-solid (VLS) growth method, first described in 1964 (*2*), has attracted overwhelming renewed attention during the past decade (*3*), as a means of producing stress-free single-crystal semiconductor nanowires with unparalleled electronic and optical properties suitable for ultraminiaturized electronics (*4*), optoelectronics (*5*), renewable energy (*6*), and chemical and biological sensing (*7*). Yet the large-scale assembly of horizontal nanowires with controlled orientation on surfaces remains a challenge toward their integration into practical devices. To this end, several assembly processes have been devised, including the use of liquid flows (*8*), electric fields (*9*),

[1]Department of Materials and Interfaces, Weizmann Institute of Science, Rehovot 76100, Israel. [2]Chemical Research Support, Weizmann Institute of Science, Rehovot 76100, Israel.

*To whom correspondence should be addressed. E-mail: ernesto.joselevich@weizmann.ac.il

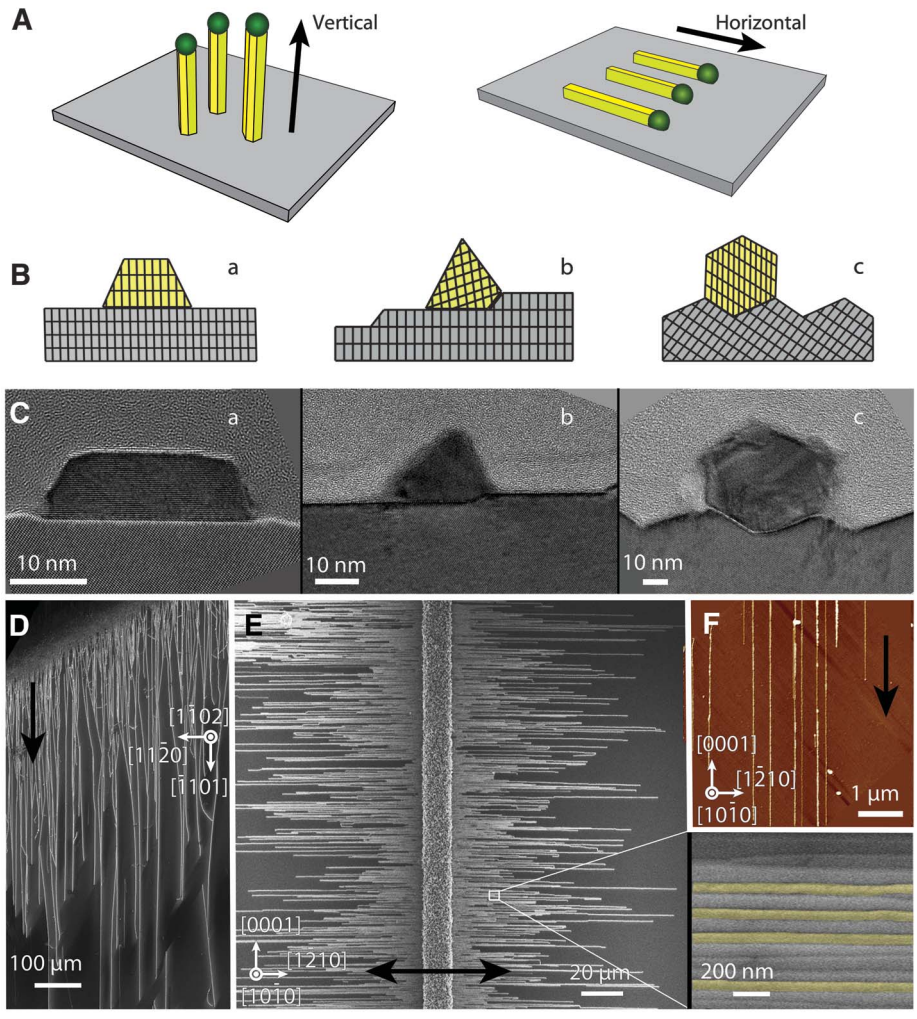

Fig. 1. Guided VLS growth of horizontal nanowires: Concept and realization. (**A**) Schematic view of guided VLS growth (right) versus conventional VLS growth (left). (**B**) Three postulated modes of guided VLS growth (schematic cross-sectional views): (a) epitaxial growth along specific lattice directions, (b) graphoepitaxial growth along L-shaped nanosteps of an annealed miscut substrate, and (c) graphoepitaxial growth along V-shaped nanogrooves of an annealed unstable low-index substrate. (**C**) Experimental realization of (B) for GaN nanowires on different planes of sapphire (cross-sectional TEM images): (a) C (0001), (b) annealed miscut C (0001) by 2° toward [$\bar{1}$100], and (c) annealed M (10$\bar{1}$0). (**D**) Ultralong (>1 mm), unidirectional GaN nanowires grown on R (1$\bar{1}$02) sapphire. (**E**) Perfectly aligned GaN nanowires grown on annealed M-plane sapphire. Detail: magnification of the dense nanowires (highlighted in yellow) along the sapphire nanofacets. (Note that nanowires in SEM images may appear broadened as a result of static charging.) (**F**) Atomic force microscope (AFM) image of unidirectional GaN nanowires grown on nonannealed M-plane sapphire.

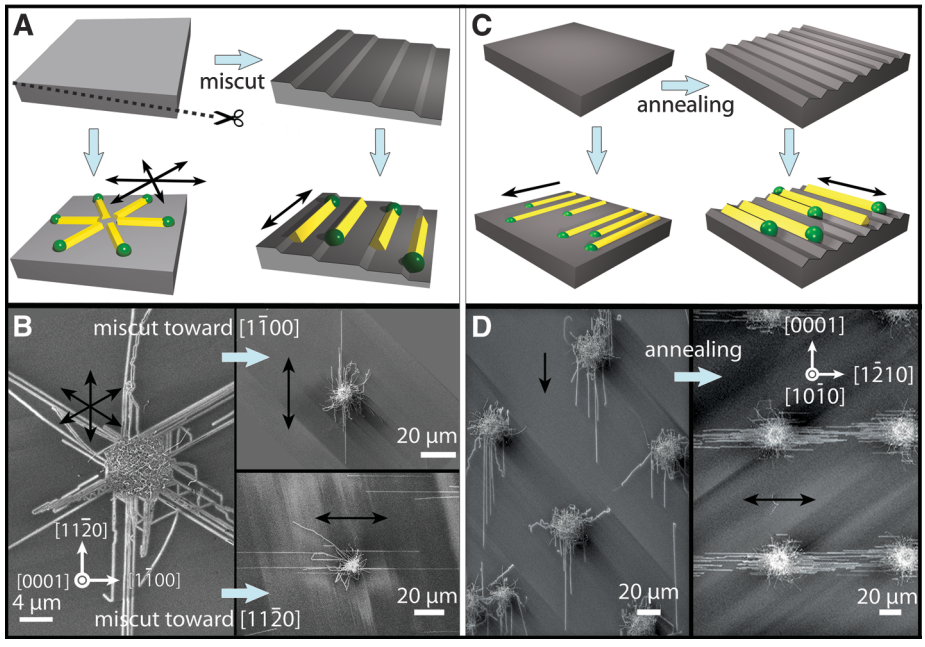

Fig. 2. Graphoepitaxial effect on the guided VLS growth of horizontal nanowires. (**A**) Graphoepitaxial effect on C-plane sapphire (schematic). (**B**) Corresponding scanning electron microscope (SEM) images showing how the guided growth of GaN nanowires changes from six directions on well-cut C plane (left side) to bidirectional growth, by the introduction of nanosteps when the substrate is miscut toward [1$\bar{1}$00] (top right) and [11$\bar{2}$0] (bottom right). (**C**) Graphoepitaxial effect on M-plane sapphire (schematic). (**D**) Corresponding SEM images showing how the guided growth changes from unidirectional (left) to bidirectional at ±90°, by the introduction of nanogrooves when the substrate is annealed (right).

Langmuir-Blodgett compression (*10*), and mechanical shear (*11*).

Although these postgrowth assembly methods yield relatively well-aligned arrays on a variety of surfaces on a wafer-scale size, their alignment is subject to thermal and dynamic fluctuations. The assembled nanowires are usually not much longer than 10 μm, and there is no control over their crystallographic orientation. VLS growth enables the production of nanowires with controlled polar or nonpolar crystallographic orientations that affect their optical and electronic properties (*12*), as well as nanowire p-n and p-i-n heterojunctions with modulated doping (*13*) and composition (*14*), suitable for electronics, optoelectronics, and photovoltaics (*15*). But when these polar nanowires and heterojunctions are collected and dispersed to be assembled, their directionalities become irreversibly scrambled.

Guided growth of horizontally aligned nanowires (Fig. 1A, right) could overcome the limitations of postgrowth assembly by combining synthesis and assembly in a single step. The guided growth of carbon nanotubes, demonstrated by our group along atomic steps (*16*) and nanosteps (*17*) of miscut C-plane sapphire, is now widely used on a variety of planes of sapphire and quartz (*18*). VLS growth of horizontally aligned semiconductor nanowires has been reported for a limited number of materials and substrates, including ZnO nanowires on A-plane sapphire (*19*) and GaAs nanowires on GaAs(100) (*20*). In both cases, the alignment was induced by a single epitaxial relationship, and hence the possibility of controllably varying the crystallographic orientation of the nanowires was not demonstrated; nor did previous work exploit the strong guiding effect of surface steps and grooves, known as "graphoepitaxy" (*21*). Overall, the guided VLS growth was not sustainable enough to produce horizontally aligned nanowires much longer than 10 μm, whereas guided growth of carbon nanotubes can yield aligned arrays longer than 1 mm.

We report the guided VLS growth of aligned, millimeter-long, horizontal GaN nanowires with controlled crystallographic orientations on several different planes of sapphire, including both atomically flat and spontaneously faceted surfaces. We focused our study on GaN because, besides its great technological importance, this material is known to possess a variety of epitaxial relationships with different planes of sapphire (*22*). This gives us an opportunity to investigate the effects of epitaxy and graphoepitaxy, acting in cooperation or in competition, to determine the orientation, morphology, atomic structure, and physical properties of horizontally grown nanowires.

We postulate three general modes of guided VLS growth of horizontal nanowires, depending on the substrate morphology, as depicted in Fig. 1B: (a) epitaxial growth along specific lattice directions, driven by minimization of interfacial energy and strain; (b) graphoepitaxial growth along L-shaped nanosteps spontaneously formed upon annealing a miscut substrate, driven by maximization of the interface area between the substrate and the nanowire or the catalyst; and (c) graphoepitaxial growth along V-shaped nanogrooves spontaneously formed upon annealing an unstable low-index surface, driven similarly to (b). Sapphire (α-Al_2O_3) is a trigonal crystal of the R$\bar{3}$c space group. Its equilibrium Wulff shape is characterized by facets C{0001}, R{1$\bar{1}$02}, S{10$\bar{1}$1}, P{11$\bar{2}$3}, A{11$\bar{2}$0}, and M{10$\bar{1}$0} (too unstable to be present), in order of increasing surface energy (*23*). Thus, when sapphire substrates with unstable orientations, such as M plane or miscut C plane, are annealed at a high temperature, they spontaneously become periodically faceted, as shown in Fig. 1B, (b) and (c), respectively (*24*).

We grew GaN nanowires on eight different planes of sapphire: C, A, R, M, annealed M, and annealed miscut C planes tilted by 2° toward [11$\bar{2}$0], [1$\bar{1}$00], and [$\bar{1}$100]. The GaN nanowires were grown by chemical vapor deposition (CVD) from Ga_2O_3 powder in a flow of N_2, H_2, and

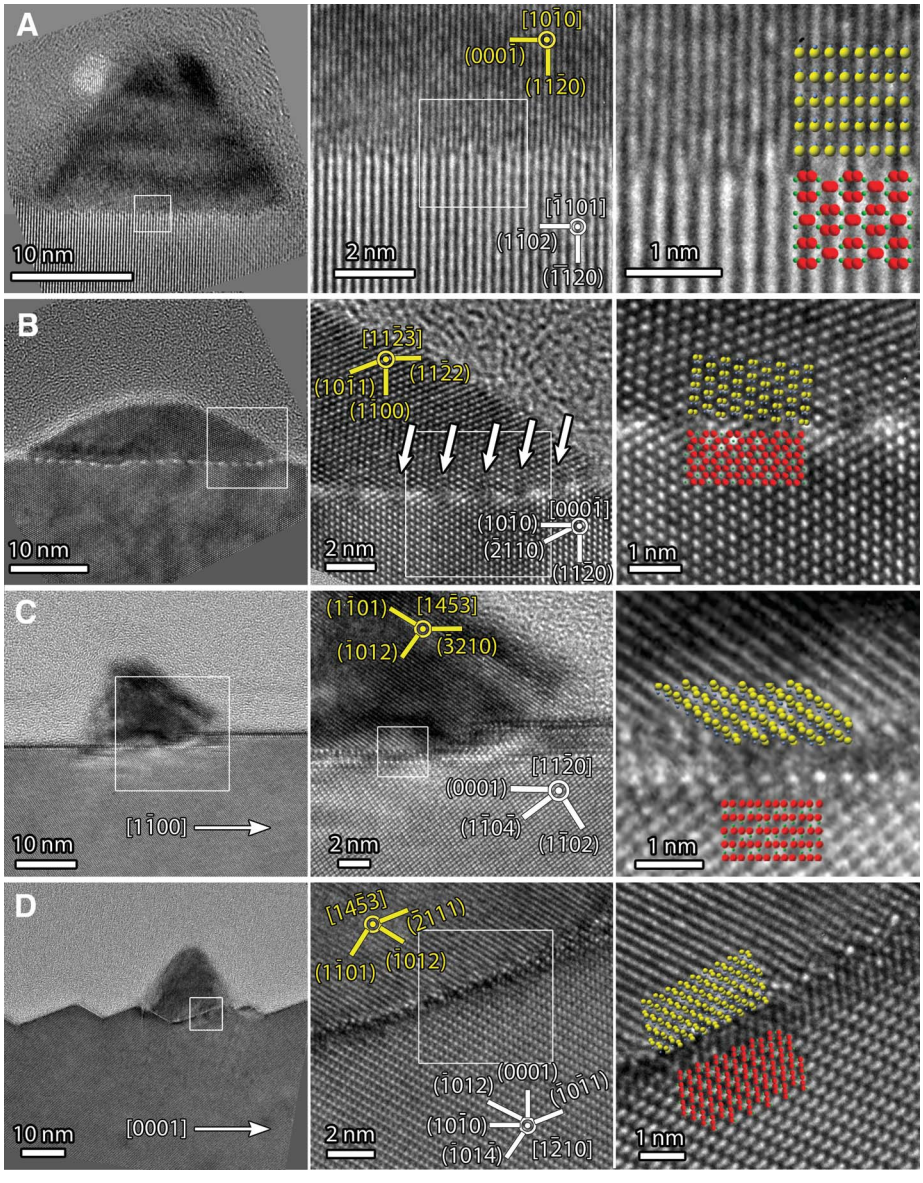

Fig. 3. Different morphologies of guided GaN nanowires (cross-sectional TEM images, white-line squares indicating the zoom areas to the right): (**A**) Perfectly matched epitaxial nanowires, exemplified by a GaN nanowire on R-plane sapphire. The nanowire and substrate fringes display a perfect 3:2 ratio with no misfit dislocations (sample slightly tilted to highlight vertical fringes). (**B**) Mismatched epitaxial nanowires, exemplified by a GaN nanowire on M-plane sapphire. The 16% lattice mismatch is released by the formation of misfit dislocations (indicated by white arrows) consistent with the 6:7 ratio between the nanowire and substrate lattice parameters in this orientation. (**C**) Graphoepitaxial nanowires along L-shaped nanosteps, exemplified by a GaN nanowire on annealed C-plane sapphire miscut 2° toward [1$\bar{1}$00]. (**D**) Graphoepitaxial nanowires along V-shaped nanogrooves, exemplified by a GaN nanowire on annealed M-plane sapphire. The atomic models on the right are consistent with fringes and TEM simulations.

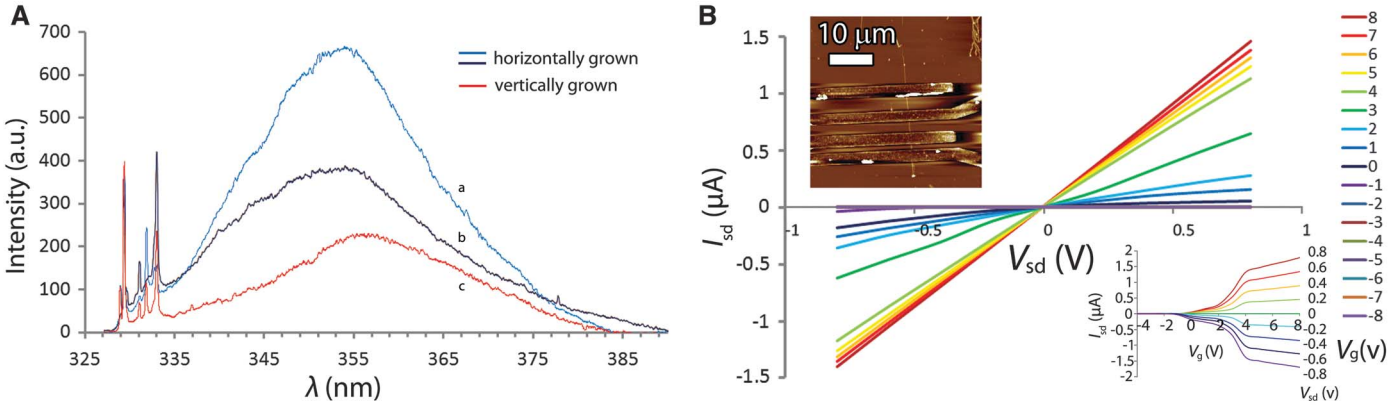

Fig. 4. Optical and electronic properties of guided GaN nanowires. (**A**) Typical room-temperature, single-nanowire photoluminescence spectra of (a) horizontally grown GaN nanowires on M-plane sapphire, (b) horizontally grown GaN nanowires on annealed C-plane miscut sapphire toward [11$\bar{2}$0], and (c) vertically grown GaN nanowires dispersed on A-plane sapphire. Excitation wavelength λ_{ex} = 325 nm. The sharp peaks at 329 to 333 nm are from Raman scattering. (**B**) Electrical characterization of guided GaN nanowires in a single-nanowire FET configuration at room temperature. Graphs of source-drain current (I_{sd}) versus source-drain voltage (V_{sd}) are displayed for different gate voltages (V_g). Upper left inset: AFM image of a typical FET device, showing the nanowire and four electrodes before deposition of the dielectric and top gate. Lower right inset: I_{sd}-V_g curves for different V_{sd} bias voltages. The charge carrier density can be extracted from the linear part of the graph (*25*). The electrical measurements were preformed on nanowires horizontally grown on R-plane and annealed M-plane sapphire, yielding similar results.

NH_3 at 950°C and 400 mbar (*25*). The catalyst consisted of Ni nanoparticles patterned as islands or stripes by photolithography. After CVD, the bulk of the catalyst stripes was covered with entangled forests of vertically grown GaN nanowires, whereas the stripe edges led to a large number of horizontal nanowires extending onto the clean sapphire surface. Sonication for a few seconds in isopropanol removed the nanowire forests, leaving only the horizontal nanowires in place.

Growth from catalyst stripes on atomically flat R-plane sapphire yielded horizontally aligned GaN nanowires longer than 1 mm (Fig. 1D), although the alignment was not perfect, whereas on annealed M-plane sapphire the nanowires were perfectly aligned with no observable deviations (Fig. 1E). The better alignment of the latter is attributed to the graphoepitaxial effect. The nanowires have a typical width of 5 to 50 nm, and their arrays can be as dense as 20 nanowires/μm.

The graphoepitaxial effect is exemplified on annealed miscut C-plane and annealed M-plane sapphire: On well-cut C-plane sapphire (Fig. 2, A and B, left), GaN nanowires formed random triangular patterns by growing along the six isomorphic ⟨11$\bar{2}$0⟩ directions defined by the threefold symmetry of the C plane and the three {11$\bar{2}$0} glide planes [contrary to (*26*), which reports growth along ⟨10$\bar{1}$0⟩]. However, when the C plane was miscut by 2° toward [1$\bar{1}$00], the GaN nanowires chose to grow only along two directions ±[11$\bar{2}$0], forming parallel arrays (Fig. 2, A and B, right). Here, the VLS growth was clearly guided by the L-shaped nanosteps, as postulated in Fig. 1B, (b). Furthermore, when the C plane was miscut by 2° toward [11$\bar{2}$0], the GaN nanowires were coerced to grow along the ±[1$\bar{1}$00] directions of the steps, at 30° from the growth directions preferred by the well-cut C plane (Fig. 2B, bottom right). Hence, graphoepitaxy overrules epitaxy. Analogously, on nonannealed M-plane sapphire, GaN nanowires grew unidirectionally along [000$\bar{1}$] (Fig. 2, C and D, left, and Fig. 1F). But when the same M-plane sapphire was annealed before CVD, the GaN nanowires switched their growth direction by ±90°, growing bidirectionally along the ±[11$\bar{2}$0] directions of the spontaneously faceted V-shaped nanogrooves (Fig. 2, C and D, right, and Fig. 1E), as postulated in Fig. 1B, (c).

We characterized the crystallographic orientation of the GaN nanowires and their epitaxial/graphoepitaxial relationship with the sapphire substrate by cutting thin (50 to 100 nm) slices across the nanowires by means of a focused-ion beam (FIB) and observing them under a high-resolution transmission electron microscope (TEM). Low-magnification images (Fig. 1C) confirmed the postulated modes of guided growth (Fig. 1B), and most nanowires displayed well-defined facets. Higher-magnification images displayed clear fringes on both the GaN and Al_2O_3, which can be identified with known crystallographic data and fit to atomic models (Fig. 3). All the GaN nanowires had a hexagonal wurtzite structure, but their morphology and orientation varied with the substrate orientation. The images in Fig. 3, A to D, exemplify guided nanowires with four different morphologies: a perfectly matched epitaxial nanowire, a mismatched epitaxial nanowire, a graphoepitaxial nanowire along an L-shaped nanostep, and a graphoepitaxial nanowire along a V-shaped nanogroove. These four cases are exemplified, respectively, on the R, M, annealed miscut C toward [$\bar{1}$100], and annealed M planes of sapphire. The growth directions, crystallographic orientations, epitaxial relationships, and faceting of these and other nanowires and substrates are described in fig. S1 and tables S1 and S2. For instance, on R-plane sapphire (Fig. 3A), the GaN nanowires usually grew in epitaxy with the $(11\bar{0}2)_{Al_2O_3}$ plane, along the $[\bar{1}101]_{Al_2O_3}$ direction, and with a nonpolar $[10\bar{1}0]_{GaN}$ orientation. These nanowires have isosceles triangular cross sections with their $(0001)_{GaN}$ face downward in epitaxy with the substrate, and $(1\bar{2}12)_{GaN}$ and $(1\bar{2}1\bar{2})_{GaN}$ facets exposed. Here the mismatch is almost negligible (0.49%), and no misfit dislocations are observed. In contrast, on M-plane sapphire (Fig. 3B) there can be a large mismatch (16%) across the nanowire axis, where the nanowire-substrate interface displays misfit dislocations every six fringes of the sapphire. This is consistent with the 6:7 ratio between the lattice parameters of the GaN and Al_2O_3 across the nanowire in this orientation. Here, the nanowire axis has a semipolar $[11\bar{2}3]_{GaN}$ orientation. On annealed miscut C plane toward [$\bar{1}$100] (Fig. 3C), the nanowires grew, as mentioned (Fig. 2C, top right), along the $\pm[11\bar{2}0]_{Al_2O_3}$ directions, namely a subset of the same directions preferred on the well-cut C plane. Surprisingly, though, the crystallographic orientation of the GaN nanowires on the miscut C plane switched from the nonpolar $[10\bar{1}0]_{GaN}$ axis preferred on the well-cut C plane to an unusual semipolar $[14\bar{5}3]_{GaN}$ axis. Thus, graphoepitaxy not only overrules the preferred epitaxial relationship, but can also induce nanowires to grow with unusual epitaxial relationships and crystallographic orientations. On annealed M-plane sapphire (Fig. 3D), the nanowires grow in epitaxial relationship with either the S- or R-plane facets of the V-shaped nanogrooves, with the same $[14\bar{5}3]_{GaN}$ axial orientation as on miscut C plane.

We performed similar analyses for more than 85 nanowires on eight different substrate orientations (figs. S1 to S16 and table S1). In general, the nanowires grew in well-defined and reproducible directions with a single crystallographic orientation, although in some cases there were

secondary epitaxial relationships leading to nanowires with other crystallographic orientations. In these cases, the axial orientation was usually similar for all the nanowires grown on each substrate, whereas the rotational orientation of the nanowires around their axis varied from one nanowire to another (table S1). This can be attributed to the fact that stress can be more easily relieved across the nanowire than along its axis. The rotational variability was especially pronounced in graphoepitaxial nanowires along V-shaped nanogrooves. This may be related to the fact that, along these faceted substrates, the nanowires must accommodate incompatible epitaxial relationships with two different facets (fig. S13). We note that the epitaxial nanowires usually prefer nonpolar axial orientations ($[10\bar{1}0]_{GaN}$ on C-, A-, and R-plane sapphire, and $[11\bar{2}0]_{GaN}$ on M-plane sapphire), whereas the graphoepitaxial nanowires tend to adopt unusual semipolar orientations such as $[14\bar{5}3]_{GaN}$ and $[1\bar{1}02]_{GaN}$. Elementary mapping of Ga, N, Al, and O by electron energy loss spectroscopy (EELS) revealed sharp GaN-Al_2O_3 interfaces without observable interdiffusion (fig. S4).

Our results show a relationship between the nanowire growth directions and the symmetry of the chosen substrate plane, as shown in fig. S1. Flat substrates with D_3, C_2, or D_1 morphological symmetries led to epitaxial nanowire growth along six directions, two directions, and one single direction, respectively. When the substrate had D_1 symmetry and the nanowires grew parallel to the only symmetry plane, as on R- and M-plane sapphire, there was no symmetry operation that could exchange between the forward and backward directions of growth. This asymmetry caused the nanowires to grow in one single direction. Such unidirectional growth has clear advantages over bidirectional growth both for polarity control and for integration purposes, because one can pattern the catalyst and have all the nanowires extending from it in the same direction (Fig. 2D, left). The photophysical properties of semiconductor nanowires and thin films were found to be affected by their polarity; this is because radiative lifetimes and quantum efficiencies are affected by changes in electron-hole overlap due to internal fields (*27*). Epitaxial VLS growth on different substrates has enabled the selective production of polar and nonpolar nanowires as vertical arrays (*12*), but no available postgrowth method based on dispersions can horizontally align them with coherent polarity, whereas guided growth could yield coherently oriented nanowires with similar polarity. This polarity control may have important advantages in photonic, optoelectronic, and radio-frequency applications, as well as in nonlinear optics (*22*).

Once the guided growth of semiconductor nanowires has been demonstrated, the next question is to what extent the horizontal epitaxial or graphoepitaxial growth may lead to stress-induced defects, which can affect the optical and electronic properties of the nanowires. We used a confocal microscope with a He-Cd laser to characterize the optical properties by single-nanowire photoluminescence (Fig. 4A). The photoluminescence spectra were typical of GaN, although with a slight blue shift (λ_{max} = 354 nm), possibly a result of quantum confinement or compressive strain (*28*), and did not show any signs of the typical "yellow tail" that is usually observed in defective GaN because of optical transitions involving in-gap states (*22*). Moreover, the photoluminescence spectra from horizontally grown nanowires were very similar to those from nanowires vertically grown in the same conditions and dispersed onto the same substrate with an even higher intensity.

Another property that may be affected by defects is the charge carrier mobility. We characterized the electronic properties of the horizontal epitaxial and graphoepitaxial GaN nanowires by building single-nanowire field-effect transistors (Fig. 4B) and thin-film transistors (fig. S17) with top gates. The nanowires displayed n-type behavior (Fig. 4B) with mobility μ = 60 to 250 $cm^2\ V^{-1}\ s^{-1}$ and electron density $n_e = 1 \times 10^{18}$ to $2 \times 10^{19}\ cm^{-3}$. These values are comparable with those reported for nonhorizontally grown GaN nanowires (*29*, *30*).

Overall, both the optical and electronic properties of horizontally grown GaN nanowires were surprisingly similar or even superior to those of nonhorizontally grown ones. This indicates that the interaction with the substrate during growth does not induce defects that degrade the optical and electronic properties of the semiconductor, as opposed to epitaxial growth of 2D films. This important difference can be attributed to the fact that in a continuous film, stress accumulates in two dimensions, whereas in a nanowire, stress accumulates only in the macroscopic axial direction and can be effectively released by contraction, expansion, or localized misfit dislocations in the transverse direction. Thus, guided VLS growth enjoys the beneficial orientation control of epitaxial growth without suffering the stress-related problems of traditional epitaxial growth in 2D layers.

The mechanism of guided VLS growth remains to be understood. A recent theoretical model predicts horizontal VLS growth of nanowires, on the basis of catalyst droplet statics and the formation and growth of nanowire facets (*31*). Although this model appears to be highly relevant to our results, as a continuum model, it does not refer to the epitaxial relationship between the nanowire material and the substrate [for further discussion, see (*25*) and figs. S18 to S20].

We believe that the guided VLS growth of nanowires, demonstrated here for GaN on sapphire, could be extended to a large variety of semiconductors and substrates, producing ordered arrays of nanowires and heterojunctions with coherently modulated composition and doping. This will enable the production of semiconductors with highly controlled structures and unique properties, suitable for a wide range of applications, including nanoscale high-power circuits, LEDs, lasers, photovoltaic cells, photodetectors, and radio-frequency, photonic, and nonlinear optical devices.

References and Notes

1. H. P. Maruska, J. J. Tietjen, *Appl. Phys. Lett.* **15**, 327 (1969).
2. R. S. Wagner, W. C. Ellis, *Appl. Phys. Lett.* **4**, 89 (1964).
3. P. D. Yang, R. X. Yan, M. Fardy, *Nano Lett.* **10**, 1529 (2010).
4. W. Lu, C. M. Lieber, *Nat. Mater.* **6**, 841 (2007).
5. R. X. Yan, D. Gargas, P. D. Yang, *Nat. Photonics* **3**, 569 (2009).
6. A. I. Hochbaum, P. D. Yang, *Chem. Rev.* **110**, 527 (2010).
7. Y. Cui, Q. Q. Wei, H. K. Park, C. M. Lieber, *Science* **293**, 1289 (2001).
8. Y. Huang, X. F. Duan, Q. Q. Wei, C. M. Lieber, *Science* **291**, 630 (2001).
9. P. A. Smith *et al.*, *Appl. Phys. Lett.* **77**, 1399 (2000).
10. S. Jin *et al.*, *Nano Lett.* **4**, 915 (2004).
11. Z. Y. Fan *et al.*, *Nano Lett.* **8**, 20 (2008).
12. T. Kuykendall *et al.*, *Nat. Mater.* **3**, 524 (2004).
13. C. Yang, Z. H. Zhong, C. M. Lieber, *Science* **310**, 1304 (2005).
14. M. S. Gudiksen, L. J. Lauhon, J. Wang, D. C. Smith, C. M. Lieber, *Nature* **415**, 617 (2002).
15. T. J. Kempa *et al.*, *Nano Lett.* **8**, 3456 (2008).
16. A. Ismach, L. Segev, E. Wachtel, E. Joselevich, *Angew. Chem. Int. Ed.* **43**, 6140 (2004).
17. A. Ismach, D. Kantorovich, E. Joselevich, *J. Am. Chem. Soc.* **127**, 11554 (2005).
18. S. J. Kang *et al.*, *Nat. Nanotechnol.* **2**, 230 (2007).
19. B. Nikoobakht, C. A. Michaels, S. J. Stranick, M. D. Vaudin, *Appl. Phys. Lett.* **85**, 3244 (2004).
20. S. A. Fortuna, J. G. Wen, I. S. Chun, X. L. Li, *Nano Lett.* **8**, 4421 (2008).
21. M. W. Geis, D. C. Flanders, H. I. Smith, *Appl. Phys. Lett.* **35**, 71 (1979).
22. H. Morkoç, *Handbook of Nitride Semiconductors and Devices* (Wiley-VCH, Weinheim, Germany, 2008), vol. 1.
23. J. H. Choi *et al.*, *J. Am. Ceram. Soc.* **80**, 62 (1997).
24. R. Gabai, A. Ismach, E. Joselevich, *Adv. Mater.* **19**, 1325 (2007).
25. See supporting material on *Science* Online.
26. Z. Wu, M. G. Hahm, Y. J. Jung, L. Menon, *J. Mater. Chem.* **19**, 463 (2009).
27. P. Waltereit *et al.*, *Nature* **406**, 865 (2000).
28. J. B. Schlager *et al.*, *J. Appl. Phys.* **103**, 124309 (2008).
29. Y. Huang, X. F. Duan, Y. Cui, C. M. Lieber, *Nano Lett.* **2**, 101 (2002).
30. T. Kuykendall *et al.*, *Nano Lett.* **3**, 1063 (2003).
31. K. W. Schwarz, J. Tersoff, *Nano Lett.* **11**, 316 (2011).

Acknowledgments: We thank L. Zeiri for assistance in PL measurements; M. Bar-Sadan and L. Houben for assistance with TEM simulations; and W. D. Kaplan, M. Baram, H. Meltzman, R. Tenne, and L. Kronik for helpful discussions and critical comments. Supported by the Israel Science Foundation, Kimmel Center for Nanoscale Science, Moskowitz Center for Nano and Bio-Nano Imaging, and the Djanogly, Alhadeff, and Perlman foundations.

Supporting Online Material

www.sciencemag.org/cgi/content/full/333/6045/1003/DC1
Materials and Methods
SOM Text
Tables S1 and S2
Figs. S1 to S20
References (*32*–*37*)

16 May 2011; accepted 11 July 2011
10.1126/science.1208455